Atmospheric Environment Vol. 20, No. 3, pp. 447–453, 1986
Printed in Great Britain.

0004–6981/86 $3.00 + 0.00

LINEAR THEORY OF THE URBAN HEAT ISLAND CIRCULATION

J. OERLEMANS
Institute of Meteorology and Oceanography, University of Utrecht, Princetonplein 5, 3508 TA Utrecht, The Netherlands

(*First received* 14 *January* 1985 *and received for publication* 2 *September* 1985)

Abstract—A linear time-dependent model of the urban heat island circulation is developed for use in situations with a marked inversion. It has the external and first-internal gravity wave modes as basic dynamic ingredients (the inversion is treated as a 'free' surface). The background wind field may vary with height and in time, and the Coriolis acceleration, though not important in most cases, is taken into account.

The model equations are formulated in two-D (horizontal) Fourier space, permitting a fully implicit scheme to be used. Large time steps can then be employed, so that the external mode is implicitly in balance, while the internal mode slowly evolves. The value of the model lies in its efficiency: with 1600 two-D Fourier components and a 1-h time step, a 10-h integration typically takes 20 s of central processor time on a Cyber 175. The model is thus suitable for use in connection with operational air quality models running on smaller computers. Another advantage over more complete mesoscale atmospheric models is that initialization is very simple.

Various examples are discussed to illustrate the performance of the model.

1. INTRODUCTION

The importance of the urban heat island circulation has been recognized for a long time, and in recent years a very large numbers of papers dealing with its observational and theoretical aspects have been published. To name a few: Clark (1969), Tyson *et al.* (1972), Angell *et al.* (1971), Oke (1973, 1984), Delage and Taylor (1970), Shreffler (1978), Hjelmfelt (1978) and Lee (1979).

It is generally agreed that two factors contribute in a significant way to temperature differences between rural and urban regions, namely (i) heat production by human activities (typically 50 $W m^{-2}$ for a large city in winter), and (ii) different radiative and thermal properties of the city, leading to another heat balance and delay effects. It depends on the time of day and the prevailing weather conditions.

From a practical point of view, the circulation generated by the heat island is of interest because of its influence on the dispersion of air pollution. Under stable and calm conditions, the urban heat island circulation becomes very important with regard to transport and mixing. Air quality models are used more and more to understand and monitor the distribution of atmospheric pollutants. Depending on the degree of sophistication, such models require meteorological input data like mixing coefficients, humidity, radiative fluxes, and large-scale wind fields. In many cases the wind field can be taken from synoptic data, and together with the temperature stratification mixing coefficients can be determined using parameterization scheme.

However, critical situations normally occur when the synoptic-scale flow is weak, and the stratification is stable. Then the locally-induced circulations come into play, and a hydrodynamic model has to be used to obtain a prediction of the wind field. Thus, any air-quality model meant to operate for such conditions should in some way be coupled to a mesoscale atmospheric model. If a sufficiently efficient model is available, runs for many different circumstances may lead to better planning. Least critical areas for industrial activities, for instance, can then be found by Monte Carlo techniques. One problem of this approach is that the 'normal' nonlinear mesoscale models are not easy to use. They require very long central processor times (so they can only be handled on large computers), and initialization is a problem in itself.

In view of this, it seems worthwhile to search for simpler models that nevertheless reproduce the essential characteristics of the urban heat island circulation for various large-scale weather conditions. In this paper an attempt is made to develop such a model. It is based on the following considerations:

(i) circulations are generally weak, so linearization around a basic state is appropriate;
(ii) in situations of interest, large-scale subsidence has caused the presence of an inversion at a low level, restricting the depth of the circulation;
(iii) the flow can be considered to be incompressible and hydrostatic;
(iv) since the inversion restricts the depth of the circulation, inflow and outflow will very quickly be found over roughly equal depths (half of the inversion height), except when the stratification varies strongly below the inversion;
(v) spectral expansion of the variables (in two-D

Fourier space) allows a fully implicit scheme to be used for time integration.

These arguments naturally lead to a two-layer model with a free surface, thus being able to support the external and first internal gravity wave mode. The basic state is uniform in the horizontal, but may change in time. In the formulation presented here the depth, background wind and thermal stratification may be different in the two layers. The effect of wind veering with height, for example, can therefore be studied.

In section 2 a simple analysis for a single Fourier component is carried out to set the stage. The results found in that calculation are not new, but show in a compact and simple way which mechanisms dampen the circulation in a significant way. It will turn out that in most situations the cooling due to upward motion over the heat source is the dominant process. It also becomes clear that the Coriolis acceleration plays an insignificant role, unless the depth of the circulation becomes of the order of a few km and the thermal stratification is weak.

The time-dependent numerical model is formulated in section 3. The basic equations in wavenumber space are given, but the method of solution is only indicated schematically. Examples of numerical experiments are discussed in section 4, and further comments concerning applicability and possible improvements are found in section 5.

2. AN ELEMENTARY CONSIDERATION OF THE HEAT ISLAND CIRCULATION

We consider a model atmosphere of height $2h$. It has two layers and the upper bound is interpreted as a free surface (see Fig. 1 for indexing of the variables). With linear exchange of momentum between the two layers, and between the lower layer and the surface, the momentum equations read (for shallow Boussinesq flow, e.g. Dutton, 1976):

$$\frac{du_1}{dt} = -\frac{1}{R^*}\left[\frac{\partial P_0}{\partial x} - \frac{1}{2}hg\frac{\partial \rho}{\partial x}\right] - k_a(u_1 - u_3) - k_b u_1 + f v_1 \tag{1}$$

$$\frac{dv_1}{dt} = -\frac{1}{R^*}\left[\frac{\partial P_0}{\partial y} - \frac{1}{2}hg\frac{\partial \rho}{\partial y}\right] - k_a(v_1 - v_3) - k_b v_1 - f u_1 \tag{2}$$

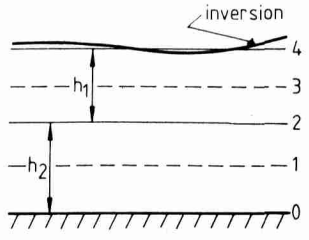

Fig. 1.

$$\frac{du_3}{dt} = -\frac{1}{R^*}\left[\frac{\partial P_0}{\partial x} - \frac{3}{2}hg\frac{\partial \rho}{\partial x}\right] - k_a(u_3 - u_1) + f v_3 \tag{3}$$

$$\frac{dv_3}{dt} = -\frac{1}{R^*}\left[\frac{\partial P_0}{\partial y} - \frac{3}{2}hg\frac{\partial \rho}{\partial y}\right] - k_a(v_3 - v_1) - f u_3. \tag{4}$$

Here u_1 and u_3 are the x-(eastward) velocities in the lower and upper layer, and v_1 and v_3 the y-(northward) velocities. R^* is a constant reference density, $\mathbf{g}$ gravitational acceleration, f Coriolis parameter, P_0 surface pressure perturbation and ρ density perturbation (assumed to be independent of height in this simple calculation).

In shallow incompressible flow, the surface pressure perturbation is linearly proportional to the vertical displacement of the upper surface relative to its equilibrium position, so

$$\frac{dp_0}{dt} = -fh\delta\left(\frac{\partial u_1}{\partial x} + \frac{\partial v_1}{\partial y} + \frac{\partial u_3}{\partial x} + \frac{\partial v_3}{\partial y}\right). \tag{5}$$

Here δ denotes the density difference across the upper surface. The density is obtained from the thermodynamic equation for shallow circulations:

$$\frac{d\rho}{dt} = -w_2\gamma - k_c(\rho - \rho_0) = h\gamma\left(\frac{\partial u_1}{\partial x} + \frac{\partial v_1}{\partial u}\right) - k_c(\rho - \rho_0) \tag{6}$$

where $$\gamma = \frac{\partial \rho^*}{\partial z} + \mathbf{g}\frac{c_v}{c_p}\frac{R^{*2}}{P^*}.$$

Forcing of the set (1) to (6) is through the surface density perturbation ρ_0. We suppose that ρ_0 is of the form $Re[Q_0 \exp(imx)]$, and search for the steady-state solution. Denoting the amplitudes of $\rho, P_0, u_1, u_3, v_1, v_3$ by Q, P, U_1, U_3, V_1, V_3, respectively, the resulting spectral equations read:

$$\frac{-im}{R^*}P + \frac{imhg}{2R^*}Q - (k_a + k_b)U_1 + k_a U_3 + fV_1 = 0 \tag{7}$$

$$-(k_a + k_b)V_1 + k_a V_3 - fU_1 = 0 \tag{8}$$

$$\frac{-im}{R^*}P + \frac{3imhg}{2R^*}Q - k_a U_3 + k_a U_1 + fV_3 = 0 \tag{9}$$

$$-k_a V_3 + k_a V_1 - fU_3 = 0 \tag{10}$$

$$imh\gamma U_1 - k_c Q + k_c Q_0 = 0 \tag{11}$$

$$U_1 + U_3 = 0. \tag{12}$$

The pressure is easily eliminated by subtracting (9) from (7). With (12) and elimination of Q through (11) we find:

$$\frac{-imhg}{R^*}Q_0 + \frac{m^2h^2g\gamma}{R^*k_c}U_1 - (4k_a + k_b)U_1 + f(V_1 - V_3) = 0. \tag{13}$$

$V_1 - V_3$ equals fU_1/k_a, so the solution of U_1 becomes:

$$U_1 = \frac{imhgQ_0/R^*}{-\frac{m^2h^2g\gamma}{R^*k_c} + 4k_a + k_b + f^2/k_a}. \quad (14)$$

Before discussing this expression we assume that all vertical mixing is of a diffusive nature, i.e. of the form $D\partial^2X/\partial z^2$, where D is diffusivity and X any dependent variable. With a finite difference approximation in the vertical, as used here, this term scales as D/h^2. For the present discussion it is therefore useful to replace k_i by D/h^2. One can argue that linear diffusion is not a very good description of mixing in atmospheric flow because it is generally turbulent. However, two points should be kept in mind. In the first place, the flow is linearized around a basic state. In practice one will therefore set the drag proportional to background velocity squared, i.e. apply larger mixing coefficients when the background flow is stronger. This essentially retains the nonlinear character of the drag. In the second place, the circulation is externally forced by a spatially varying heat flux. The complexity of the solution probably depends more on the irregularity of the forcing than on nonlinear effects. Thus, it is doubtful whether a nonlinear treatment of the secondary (i.e. heat island) flow will lead to a significant improvement, in view of the much more expensive numerical techniques that would be required.

At this point, we assume all diffusivities to be equal for simplicity. Scaling U_1 with D/h, the nondimensional solution can be written as

$$\tilde{U}_1 = U_1\frac{h}{D} = \frac{-imh^4gQ_0/(5R^*D^2)}{-\frac{m^2h^6g\gamma}{5R^*D^2} + \frac{h^4f^2}{5D^2} + 1}. \quad (15)$$

First, it is obvious that u_1 is always 90° out of phase with respect to ρ_0. Since, for a stable stratification, γ is negative, all terms in the denominator of (15) are positive and thus represent damping mechanisms to the thermally induced circulation. These mechanisms are adiabatic cooling over the heat source, reduction of inflow by the Coriolis acceleration, and diffusion (= 1 because the diffusive time scale is in fact used to nondimensionalize time). The relative importance of these factors depends on the depth of the circulation $2h$, the wavelength $L = 2\pi/m$, and the diffusivity D. It is instructive to consider this in somewhat more detail.

We first have a look at the reduction of inflow by the Coriolis acceleration. Table 1 shows values of $2h$ for which the term $h^4f^2/(5D^2)$ equals 1, for $f = 10^{-4}\,s^{-1}$. Apparently, when the urban heat island circulation is only a few hundreds of meters deep, the Coriolis acceleration plays an unimportant role. The ratio of the Coriolis effect to the stratification effect is

$$-m^2h^2g\gamma/(R^*f^2). \quad (16)$$

For typical conditions for an urban heat island circulation, it turns out that this non-dimensional number is of the order 10–100 (with $L = 20$ km, $h = 400$ m, $\gamma = 10^{-5}$ kg m^{-4}, for example, we find 156). So in most cases the stratification will be the most important limiting factor, and the solution for U_1 is:

Table 1. Depth ($2h$) of the heat island circulation for which the stabilizing effects of vertical mixing and Coriolis acceleration are equally large

D (m^2 s^{-1})	$2h$ (m)
0.1	95
0.5	210
1	300
5	668
10	944
25	1494

The Coriolis parameter was set to $10^{-4}\,s^{-1}$.
$k_i = f/\sqrt{5}$.

$$U_1 = \frac{-iQ_0D}{mh^3\gamma}. \quad (17)$$

In practice h will be half of the inversion height, and D decreases with increasing stability. So stronger circulations are expected when the stratification is less stable, the inversion is low, and when the horizontal scale of the heat source is large.

It should be noted that the Coriolis acceleration does not dampen the motion but simply turns the wind vector. It can easily be shown that the mean kinetic energy equals:

$$KE = \frac{1}{8}R^*U_1^2(2 + f^2/k_a^2). \quad (18)$$

So, irrespective of the effect of the stratification, the Coriolis acceleration will lead to large values of KE when k_a is small compared to f.

The analysis carried out here is of course very schematic. A single Fourier component does not adequately resolve the forcing associated with an urban heat island. Also, the effect of background flow has not been taken into account. One should regard this model as the simplest one possible that still reveals the basic dependence of the urban heat island circulation on such factors as stability, vertical mixing, horizontal scale and inversion height.

3. A LINEAR MODEL WITH BACKGROUND FLOW

In this section a model is developed which is time-dependent, has any desired horizontal resolution and describes the perturbation circulation relative to a mean state. The vertical configuration is the same as in the preceding section, except for the density field, which is now calculated at level 1 and level 3. The mean state is characterized by u_1^*, v_1^*, u_3^*, v_3^*, R_1^*, R_3^*, γ_1^* and γ_3^*. Note that the background flow is thus allowed to turn with height. The formulation will also be some-

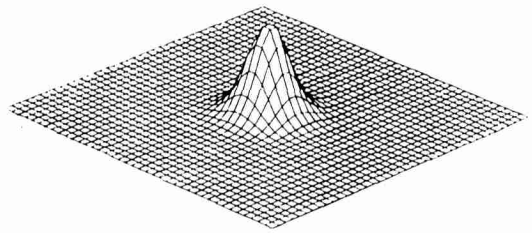

Fig. 2.

what more general by using different thicknesses for the layers 0–2 (h_1) and 2–4 (h_3).

To make an efficient integration in time possible, an implicit scheme, allowing large time steps, will be employed. For a domain of N to N grid points, this leaves us with $14 \times N^2$ linear equations that have to be solved simultaneously. However, by solving the equations in Fourier space this problem is reduced to solving a set of 14 equations N^2 times. For practical applications, a time step of 30 or 60 min will be used, which implies that the external mode is to a large extent in balance with the forcing while the internal mode is slowly evolving. The formulation given below is for a reference state that is uniform over the domain. The reference state may change in time, however.

The model equations read:

$$\frac{\partial u_1}{\partial t} + u_1^* \frac{\partial u_1}{\partial x} + v_1^* \frac{\partial u_1}{\partial y} = f v_1 - \frac{1}{R_1^*} \frac{\partial p_0}{\partial x} + \frac{g h_1}{2R_1^*} \frac{\partial \rho_1}{\partial x} - k_a(u_1 - u_3) - k_b u_1 \quad (19)$$

$$\frac{\partial v_1}{\partial t} + u_1^* \frac{\partial v_1}{\partial x} + v_1^* \frac{\partial v_1}{\partial y} = -f u_1 - \frac{1}{R_1^*} \frac{\partial p_0}{\partial y} + \frac{g h_1}{2R_1^*} \frac{\partial \rho_1}{\partial y} - k_a(v_1 - v_3) - k_b v_1 \quad (20)$$

$$\frac{\partial u_3}{\partial t} + u_3^* \frac{\partial u_3}{\partial x} + v_3^* \frac{\partial u_3}{\partial y} = f v_3 - \frac{1}{R_3^*} \frac{\partial p_0}{\partial x} + \frac{g h_1}{R_3^*} \frac{\partial \rho_1}{\partial x} + \frac{g h_3}{2R_3^*} \frac{\partial \rho_3}{\partial x} - k_a(u_3 - u_1) \quad (21)$$

$$\frac{\partial v_3}{\partial t} + u_3^* \frac{\partial v_3}{\partial x} + v_3^* \frac{\partial v_3}{\partial y} = -f u_3 - \frac{1}{R_3^*} \frac{\partial p_0}{\partial y} + \frac{g h_1}{R_3^*} \frac{\partial \rho_1}{\partial y} + \frac{g h_3}{2R_3^*} \frac{\partial \rho_3}{\partial y} - k_a(v_3 - v_1) \quad (22)$$

$$\frac{\partial \rho_1}{\partial t} + u_1^* \frac{\partial \rho_1}{\partial x} + v_1^* \frac{\partial \rho_1}{\partial y} + w_1 \gamma_1^* = -k_a(\rho_1 - \rho_3) - k_b(\rho_1 - \rho_0) \quad (23)$$

$$\frac{\partial \rho_3}{\partial t} + u_3^* \frac{\partial \rho_3}{\partial x} + v_3^* \frac{\partial \rho_3}{\partial y} + w_3 \gamma_3^* = -k_a(\rho_3 - \rho_1) \quad (24)$$

$$\frac{\partial p_0}{\partial t} + u_3^* \frac{\partial p_0}{\partial x} + v_3^* \frac{\partial p_0}{\partial y} = -g \delta h_1 \left(\frac{\partial u_1}{\partial x} + \frac{\partial v_1}{\partial y} \right) - g \delta h_3 \left(\frac{\partial u_3}{\partial x} + \frac{\partial v_3}{\partial y} \right). \quad (25)$$

Each dependent variable is now expanded in a two-D Fourier series with time-dependent coefficients. Splitting the coefficients (denoted by capitals) in real (suffix R) and imaginary (suffix i) parts, a set of 14 equations is obtained for each Fourier component (m, n). These equations are:

$$\frac{dU_{1R}}{dt} - (mu_1^* + nv_1^*)U_{1i} + (k_a + k_b)U_{1R} - fV_{1R} - \frac{m}{R_1^*} P_{0i} + \frac{mgh_1}{2R_1^*} R_{1i} - k_a U_{3R} = 0 \quad (26)$$

$$\frac{dU_{1i}}{dt} + (mu_1^* + nv_1^*)U_{1R} + (k_a + k_b)'U_{1i} - fV_{1i} + \frac{m}{R_1^*} P_{0R} - \frac{mgh_1}{2R_1^*} R_{1R} - k_a U_{3i} = 0 \quad (27)$$

$$\frac{dV_{1R}}{dt} - (mu_1^* + nv_1^*)V_{1i} + (k_a + k_b)V_{1R} + fU_{1R} - \frac{n}{R_1^*} P_{0i} + \frac{ngh_1}{2R_1^*} R_{1i} - k_a V_{3R} = 0 \quad (28)$$

$$\frac{dV_{1i}}{dt} + (mu_1^* + nv_1^*)V_{1R} + (k_a + k_b)V_{1i} - fU_{1i} + \frac{n}{R_1^*} P_{0R} - \frac{ngh_1}{2R_1^*} R_{1R} - k_a V_{3i} = 0 \quad (29)$$

$$\frac{dU_{3R}}{dt} - (mu_3^* + nv_3^*)U_{3i} + k_a U_{3R} - fV_{3R} - \frac{m}{R_3^*} P_{0i} + \frac{mgh_1}{R_3^*} R_{1i} + \frac{mgh_3}{2R_3^*} R_{3i} - k_a U_{1R} = 0 \quad (30)$$

$$\frac{dU_{3i}}{dt} + (mu_3^* + nv_3^*)U_{3R} + k_a U_{3i} - fV_{3i} + \frac{m}{R_3^*} P_{0R} - \frac{mgh_1}{R_3^*} R_{1R} - \frac{mgh_3}{2R_3^*} - k_a U_{1i} = 0 \quad (31)$$

$$\frac{dV_{3R}}{dt} - (mu_3^* + nv_3^*)V_{3i} + k_a V_{3R} + fU_{3R} - \frac{n}{R_3^*} P_{0i} + \frac{ngh_1}{R_3^*} R_{1i} + \frac{ngh_3}{2R_3^*} - k_a V_{1R} = 0 \quad (32)$$

$$\frac{dV_{3i}}{dt} + (mu_3^* + nv_3^*)V_{3R} + k_a V_{3i} + fU_{3i} + \frac{n}{R_3^*} P_{0R} - \frac{ngh_1}{R_3^*} R_{1R} - \frac{ngh_3}{2R_3^*} - k_a V_{1i} = 0 \quad (33)$$

$$\frac{dR_{1R}}{dt} - (mu_1^* + nv_1^*)R_{1i} + (k_a + k_b)R_{1R} - k_a R_{3R} + \frac{1}{2}\gamma_1^*(mU_{1i} + nV_{1i}) = k_b R_{0R} \quad (34)$$

$$\frac{dR_{1i}}{dt} + (mu_1^* + nv_1^*)R_{1R} + (k_a + k_b)R_{1i} - k_a R_{3i} - \frac{1}{2}\gamma_1^*(mU_{1R} + nV_{1R}) = k_b R_{0i} \quad (35)$$

$$\frac{dR_{3R}}{dt} - (mu_3^* + nv_3^*)R_{3i} + k_a R_{3R} - k_a R_{1i} + \gamma_3^*[h_1(mU_{1i} + nV_{1i}) + \frac{1}{2}h_3(mU_{3i} + nV_{3i})] = 0 \quad (36)$$

$$\frac{dR_{3i}}{dt} + (mu_3^* + nv_3^*)R_{3R} + k_a R_{3i} - k_a R_{1i} - \gamma_3^*[h_1(mU_{1R} + nV_{1R}) + \frac{1}{2}h_3(mU_{3R} + nV_{3R})] = 0 \quad (37)$$

$$\frac{dP_{0R}}{dt} - (mu_3^* + nv_3^*)P_{0i} = -g\delta[h_1(mU_{1i} + nV_{1i}) + h_3(mU_{3i} + nV_{3i})] \quad (38)$$

$$\frac{dP_{0i}}{dt} + (mu_3^* + nv_3^*)P_{0R} = -g\delta[h_1(mU_{1R} + nV_{1R}) + h_3 mU_{3i} + nV_{3R})]. \quad (39)$$

The simple Euler backward scheme is now used to integrate in time. So, for any equation $dX_i/dt = f(X_1, \ldots, X_{14})$ we have:

$$X_i^{(t+\Delta)} = X_i^{(t)} + \Delta f(X_1^{(t+\Delta)}, \ldots, X_{14}^{(t+\Delta)}). \quad (40)$$

The timestep is indicated with Δ. For each Fourier component we thus have a set of equations of the form:

$$M\mathbf{X}^{(t+\Delta)} = F(\mathbf{X}^t, \text{forcing}). \quad (41)$$

This set has to be solved to obtain the values of the variables one time step ahead. The right hand side is formed by the 'old' values of the variables, to which the external forcing is added. The solution is now easily obtained by inverting the matrix M. When the background state is constant in time, the matrix is also constant and has to be inverted only once for each Fourier component. Although it is not the intention to go into technical details here, it is worthwhile noting that the most efficient procedure is to integrate one component for the entire integration time, store the results and then deal with the next component. This minimizes central memory and processor time requirements. To give an order of magnitude: on a grid of 1600 points and for a basic state independent of time, a 12-h integration requires about 60 kw memory and 20 s central processor time on a Cyber-175. This applies to a 1-h time step, which should in practically all cases be sufficiently accurate.

In view of this the model has a great potential for use on a routine basis for urban areas in situations where the atmosphere is stably stratified and air pollution models are run. In such situations calculated velocity fields can be valuable input. Compared to the more complicated and much more expensive nonlinear mesoscale models, the linear model presented here is very simple in use because the initialization problem hardly exists.

4. EXAMPLES

All experiments described here were carried out on a grid of 1600 points, covering an area of 100 × 100 km. (See Fig. 2. for the shape of the forcing function.) In the first experiments the following model parameters were used: $\gamma_1^* = \gamma_2^* = -10^{-5}\,\text{kg m}^{-4}$ (corresponding to a lapse rate of slightly more than 2 kg km^{-1} less than the dry adiabatic), $h_1 = h_2 = 200$ m, $f = 10^{-4}\,\text{s}^{-1}$, $k_a = k_b = 0.25 \times 10^{-3}\,\text{s}^{-1}$, $\delta = 0.02\,\text{kg m}^{-3}$ (corresponding to a potential temperature jump of about 5 K across the inversion), $Q_0 = 0.02\,\text{kg m}^{-3}$ (maximum surface temperature in the centre of the urban region of about 5 K). A large number of experiments were carried out to investigate the effect of varying these parameters, and it turned out that the steady-state results were very similar to those obtained with the simple analytic model described in section 2 (i.e. the dependence of the amplitude of the circulation on stratification, exchange coefficients and depth of the circulation). In this section we therefore concentrate on the influence of background flow and on transient effects.

In a first experiment the background flow was independent of height, namely, $u_1^* = u_3^* = 1\,\text{m s}^{-1}$ and $v_1^* = v_3^* = 0$. When the model is run to a steady state, which is approached very closely after only 2 h of simulated time, the lower-level flow pattern of Fig. 3 shows up. The total velocity is shown, and typical velocities associated with the heat-island circulation are of the order of 1 m s^{-1}. The zone of maximum convergence is found downstream of the centre of the heat source (black spot), of course, and from the fact that the velocity field is symmetric around $y = 50$ km it is obvious that the Coriolis acceleration plays an insignificant role.

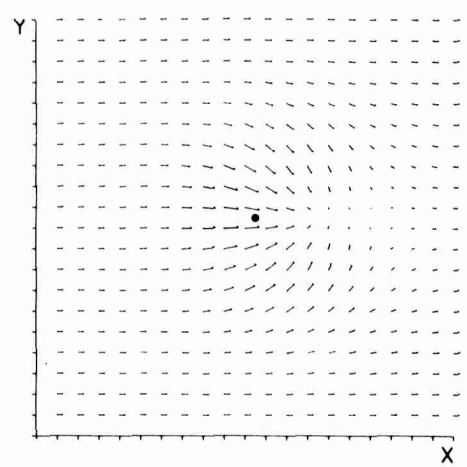

Fig. 3.

The experiment was repeated for other values of the background flow. As expected, the circulation pattern is shifted downstream and becomes weaker when the strength of the background wind increases. In terms of the mean kinetic energy

$$KE = \frac{1}{S}\int_S (u_1^2 + u_3^2 + v_1^2 + v_3^2)\,\mathrm{d}S, \qquad (42)$$

where S is the model domain, the decrease in efficiency of the circulation is not dramatic, however. For background flows of 0, 1 and 5 $\mathrm{m\,s^{-1}}$, values for KE are 0.115, 0.099 and 0.057 $\mathrm{m^2\,s^{-2}}$, respectively.

Results from an experiment with a background flow changing strongly with height are shown in Figs 4 and 5. In this case, $u_1^* = 1$, $v_1^* = 0$, $u_3^* = 0$ and $v_3^* = -4\ \mathrm{m\,s^{-1}}$. It is interesting to see that the heat-island flow pattern is displaced in a SE direction, in spite of the fact that the vertical mean background flow is almost northerly. Corresponding fields of the surface pressure perturbation and density perturbation (at level 1) are displayed in Fig. 5. The density perturbation is almost axially symmetric with a slightly displaced centre, while the pressure field is elongated towards the S. This can be understood by realizing that perturbations in the elevation of the 'free' surface are advected by the upper-level background flow.

We now consider an example of a circulation in which the Coriolis acceleration is important. As demonstrated in the analysis of section 2, this is the case when the depth of the circulation is sufficiently large, and the atmospheric stability sufficiently small. A situation in which rotational effects are not negligible is for example obtained by setting $h_1 = h_3 = 1000$ m, $\gamma^* = -0.5 \times 10^{-5}\ \mathrm{kg\,m^{-4}}$, $k_a = k_b = 5 \times 10^{-5}\ \mathrm{s^{-1}}$. The forcing, switched on suddenly at $t = 0$, is the same as in the previously discussed experiments. In this run there is no background wind.

Rotational effects can best be made visible by looking at one component of the velocity field. In Fig. 6 the x-component of the lower-level flow (u_1), in $\mathrm{cm\,s^{-1}}$, is shown for $t = 0.5$, 1, 3 and 5 h of simulated time. The effect of the Coriolis acceleration shows up as a turning of the dipole pattern. It is interesting to note that overshooting occurs in the amplitude of u_1. After 3 h, maximum velocities decrease somewhat, while the symmetry axes are still slowly turning in anticlockwise direction. The y-component of the velocity is not shown, because it is identical to the x-component, except for a rotation over 90°.

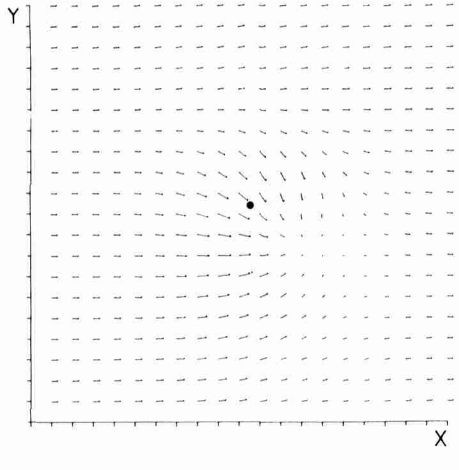

Fig. 4.

5. FINAL REMARKS

The examples given above are simple and just meant to illustrate the behaviour of the model. To run the model in an operational mode, one can envisage the following sequence of steps:

(i) Determination of the inversion height to estimate h, as well as the temperature change over the inversion to estimate δ.

(ii) Determination of the background flow and stratification for the two layers. From these quantities an estimate of the appropriate mixing coefficients can be made. A possibility would be to take the approach of Louis (1979), who presents a scheme for the calculation of mixing coefficients in dependence of wind shear and stratification.

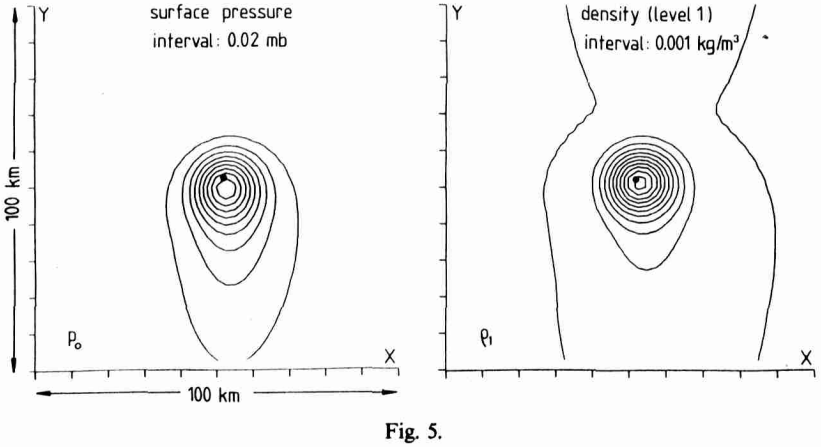

Fig. 5.

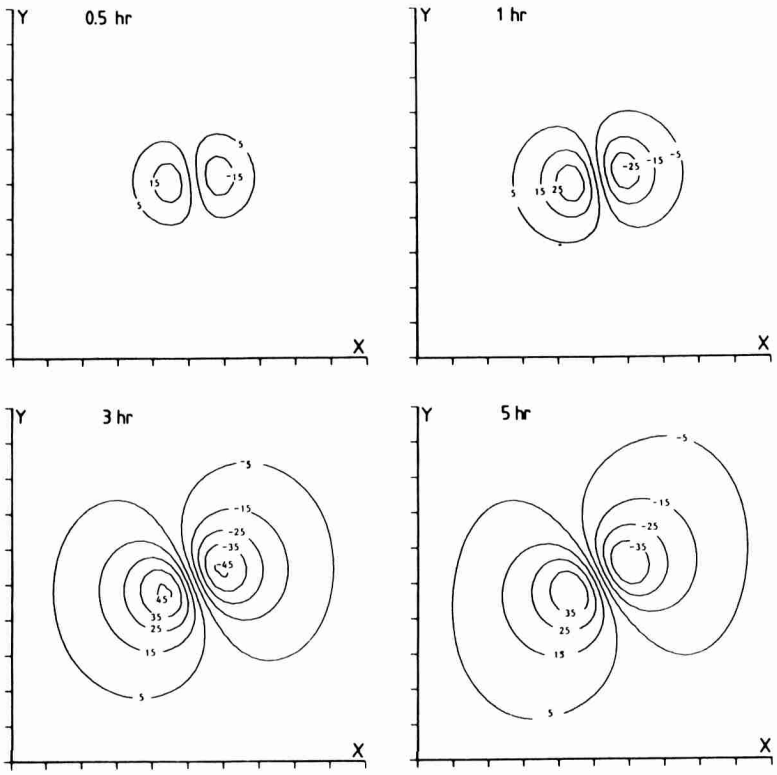

Fig. 6.

(iii) Prescription of the forcing at the surface, as a function of time when required, and decomposition of the forcing into a two-D Fourier series.

(iv) Integration of the equations for each component and storing of the results.

(v) Composition of the velocity (and, if required, other) fields from the stored Fourier coefficients.

The output can then be used for air pollution models in which advection of contaminants is taken into account.

When running the model for a specific heat island, one should realize that the boundary conditions are cyclic. A proper simulation thus requires that the size of the model domain is substantially larger than the horizontal scale of the heat-island circulation. This also implies that the domain size should be taken somewhat larger when the background flow is stronger.

The model presented here could be extended in several ways. Firstly, the number of levels could be increased to achieve a better vertical resolution of the circulation. Every additional level introduces six equations. In the formulation described in this paper a 14 × 14 matrix has to be inverted 1600 times (for each Fourier component), for a four-level model, for instance, one has to deal with 26 × 26 matrices. Another possible improvement could be the inclusion of non-linear effects. The most important one probably is the modification of the vertical exchange coefficients by the changing stratification. This can be handled by first integrating the linear system in time with constant mixing coefficients, and then rerunning the prediction by specifying new mixing coefficients in dependence of the calculated temperature field in the previous run. The effect of the change in mixing coefficients is best introduced as additional forcing, i.e. in the right-hand side of the appropriate equations.

REFERENCES

Angell J. K., Pack D. H., Dickson C. R. and Hoecker (1971) Urban influence on night-time air flow estimated from tetroon flights. *J. appl. Met.* **10,** 194–204.

Clark J. F. (1969) Nocturnal urban boundary layer over Cincinatti, Ohio. *Mon. Weath. Rev.* **97,** 582–589.

Delage Y. and Taylor P. A. (1970) Numerical studies of heat island circulations. *Boundary-Layer Met.* **1,** 423–441.

Dutton J. A. (1976) *The Ceaseless Wind.* McGraw-Hill.

Hjelmfelt M. R. (1978) Numerical simulation of the effects of St. Louis on mesoscale boundary-layer airflow and vertical air motion: simulations of urban vs non-urban effects. *J. appl. Met.* **21,** 1239–1257.

Lee D. O. (1979) The influence of atmospheric stability on the urban heat island and urban–rural wind speed differences. *Atmospheric Environment* **13,** 1175–1180.

Louis J. F. (1979) A parametric model of vertical eddy fluxes in the atmosphere. *Boundary-Layer Met.* **17,** 187–202.

Oke T. R. (1973) City size and the urban heat island. *Atmospheric Environment* **7,** 769–779.

Oke T. R. (1984) The energetic basis of the urban heat island. *Q. Jl R. met. Soc.* **108,** 1–24.

Shreffler J. H. (1978) Detection of centripetal heat island circulations from tower data in St. Louis *Boundary-Layer Met.* **15,** 229–242.

Tyson P. D., Du Toit W. J. F. and Fuggle R. F. (1972) Temperature structure above cities: review and preliminary findings from the Johannesburg urban heat island project. *Atmospheric Environment* **6,** 533–542.